Seven years of postseismic deformation following the 2003 Mw = 6.8 Zemmouri earthquake (Algeria) from InSAR time series

Esra Cetin, Mustapha Meghraoui, Ziyadin Cakir, Ahmet Akoglu, Omar Mimouni, Mouloud Chebbah

Seven years of postseismic deformation following the 2003 Mw = 6.8 Zemmouri earthquake (Algeria) from InSAR time series

Esra Cetin,[1,2] Mustapha Meghraoui,[2] Ziyadin Cakir,[1] Ahmet M. Akoglu,[3] Omar Mimouni,[4] and Mouloud Chebbah[5]

Received 13 February 2012; revised 18 April 2012; accepted 21 April 2012; published 24 May 2012.

[1] We study the postseismic surface deformation of the Mw 6.8, 2003 Zemmouri earthquake (northern Algeria) using the Multi-Temporal Small Baseline InSAR technique. InSAR time series obtained from 31 Envisat ASAR images from 2003 to 2010 reveal sub-cm coastline ground movements between Cap Matifou and Dellys. Two regions display subsidence at a maximum rate of 2 mm/yr in Cap Djenet and 3.5 mm/yr in Boumerdes. These regions correlate well with areas of maximum coseismic uplifts, and their association with two rupture segments. Inverse modeling suggest that subsidence in the areas of high coseismic uplift can be explained by afterslip on shallow sections (<5 km) of the fault above the areas of coseismic slip, in agreement with previous GPS observations. The earthquake impact on soft sediments and the ground water table southwest of the earthquake area, characterizes ground deformation of non-tectonic origin. The cumulative postseismic moment due to 7 years afterslip is equivalent to an Mw 6.3 earthquake. Therefore, the postseismic deformation and stress buildup has significant implications on the earthquake cycle models and recurrence intervals of large earthquakes in the Algiers area. **Citation:** Cetin, E., M. Meghraoui, Z. Cakir, A. M. Akoglu, O. Mimouni, and M. Chebbah (2012), Seven years of postseismic deformation following the 2003 Mw = 6.8 Zemmouri earthquake (Algeria) from InSAR time series, *Geophys. Res. Lett.*, *39*, L10307, doi:10.1029/2012GL051344.

1. Introduction

[2] Understanding the crustal deformation and earthquake cycle requires the analysis of postseismic deformation, a transient response of the lithosphere to the stress changes caused by moderate to large earthquakes. The 21 May 2003 Zemmouri earthquake and related coseismic rupture (Mw 6.8) in the Tell Atlas of northern Algeria is a motivating case study of postseismic deformation associated with a thrust faulting event. This seismic event is the largest earthquake of the last decade that can be studied with space geodesy in the Tell Atlas fold and thrust belt. Most of seismic and geodetic studies suggest a N60°–65° trending fault rupture, dipping 40° to 50° SE and located offshore about 8–13 km from the coastline [*Delouis et al.*, 2004; *Meghraoui et al.*, 2004; *Ayadi et al.*, 2008; *Mahsas et al.*, 2008; *Belabbes et al.*, 2009].

[3] Following the 2003 Zemmouri earthquake, the study of continuous GPS (CGPS) measurements at 6 benchmarks gave evidence of <1 cm/yr postseismic deformation during 2.5 years [*Mahsas et al.*, 2008]. The CGPS data can be best explained with shallow slip patches (<7.5-km-depth) with up to 30 cm afterslip, equivalent to an earthquake with moment magnitude of Mw 6.3. In this paper, to obtain a better picture of the postseismic surface deformation during 7 years, we use Small Baseline InSAR (SBI) technique with Envisat SAR data acquired by the European Space Agency. The mean velocity field deduced from the SBI reveals surface deformation of both tectonic and non-tectonic origin. We model the ground deformation along the coastal region with afterslip on the coseismic fault, and discuss the coseismic/postseismic deformation and the role of poro-elastic/visco-elastic deformation.

2. Seismotectonic Setting

[4] The 21 May 2003 Zemmouri earthquake (Mw 6.8) occurred in the Tell Atlas of northern Algeria that results from the 5–6 mm/yr present day rate of convergence between Africa and Eurasia [*Nocquet and Calais*, 2004]. The region is the source of frequent large and moderate seismic events mostly with thrust fault mechanisms in agreement with the regional tectonics [*Morel and Meghraoui*, 1996]. In north-central Algeria, the dominant active tectonic structures are NE-SW to E-W trending fold and thrust system including the Blida thrusts, Mitidja Basin and Sahel anticline (Figure 1) [*Maouche et al.*, 2011]. The 2003 earthquake ruptured ~15-km-wide crust, and caused 55-km-long coastline uplift. The coseismic uplift was ~0.5 m along the coastline, reaching a maximum 0.75 m east of Boumerdes and minimum near Cap Djenet [*Meghraoui et al.*, 2004]. Taking into account the size of coseismic slip, the investigation of postseismic deformation using satellite geodesy became suitable.

3. InSAR Data Processing and Analysis

[5] We use the Multi-temporal SBI technique of the software package StaMPS (see details of processing procedure in *Hooper* [2008]) using the ROI-PAC [*Rosen et al.*, 2004] for focusing the raw ASAR images, and the DORIS [*Kampes and Usai*, 1999] for calculating the interferograms with 90-m SRTM data. The technique minimizes the perpendicular, temporal and Doppler baselines for maximizing

[1]Department of Geology, Istanbul Technical University, Istanbul, Turkey.
[2]Institut de Physique du Globe, CNRS-UMR 7516, Strasbourg, France.
[3]Division of Physical Sciences and Engineering, King Abdullah University of Science and Technology, Thuwal, Saudi Arabia.
[4]FSTGAT, Université des Sciences et Techniques Houari Boumediene, Algiers, Algeria.
[5]Agence National des Ressources Hydrauliques, Blida, Algeria.

Corresponding author: E. Cetin, Institut de Physique du Globe, CNRS-UMR 7516, 5, rue René Descartes, F-67084 Strasbourg CEDEX, France. (e.cetin@unistra.fr)

0094-8276/12/2012GL051344

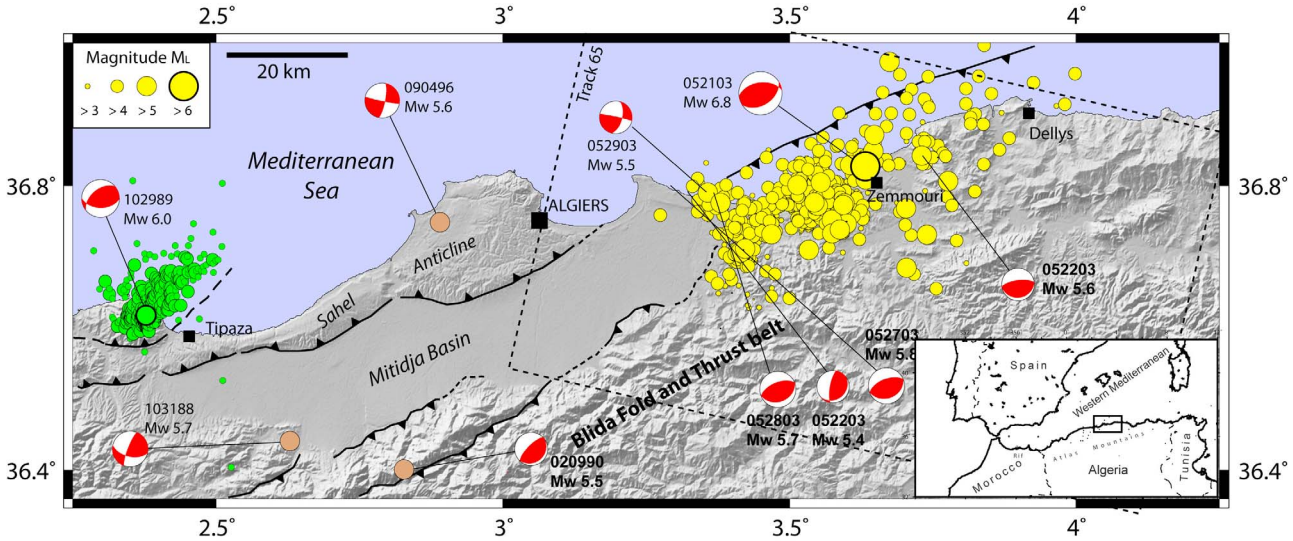

Figure 1. Tectonics and seismicity of the Zemmouri-Boumerdes region shown with SRTM shaded topography. Focal mechanisms are from Global CMT project. Two destructive earthquakes and related aftershocks (Mont Chenoua-Tipasa 1989 and Zemmouri 2003, green and yellow circles, respectively) limit the Mitidja-Algiers active zone (black lines are thrust faults [*Maouche et al.*, 2011]). Dashed box is the Envisat image frame (Track 65). Black box in inset map shows the study region.

the correlation of generated interferograms and increasing the number of observable ground points [*Berardino et al.*, 2002].

[6] A map of cumulative Line of Sight (LOS) displacements between 12-July-2003 and 18-September-2010 is obtained from a mean LOS velocity field calculated from about 86,000 coherent pixels identified in 31 descending ENVISAT images covering the earthquake region (Figure 2a). The map reveals range increase largely in three regions reaching 12 mm/yr in the Mitidja basin, 3.5 mm/yr around Boumerdes, and 2 mm/yr around Cap Djenet (Figures 2a and 2b). Range increase in the descending imaging geometry can be due to either ground subsidence or westerly horizontal ground motion. While the high rate of range increase in the Mitidja basin SW of Cap Matifou can be attributed to subsidence due to excess ground water extraction in Holocene fine-grained alluvial deposits [*Mimouni*, 2010], those observed in the earthquake coastal region are likely due to both horizontal and vertical displacements associated with the postseismic deformation, the basements of these regions being mainly formed by solid rocks (e.g., granitic and volcanic units). Although the range increase in Boumerdes area is consistent with the CGPS measurements showing both subsidence and northwestward horizontal slip, the CGPS results with large component of uplift and range decrease in Cap Djenet (CDJP) [*Mahsas et al.*, 2008] contradicts with the InSAR range increase results. As for the coseismic uplift, the postseismic ground deformation in Boumerdes and Cap Djenet must result from crustal deformation; this inference may be supported by the logarithmic decay in InSAR time series (Figure 2b). The correlation between InSAR time series and water level piezometric changes due to seasonal water level fluctuation and ground water extraction (Figure 2b) [*Mimouni*, 2010] supports the evidence for subsidence in the Mitidja basin.

[7] Although much smaller, the sense of postseismic range change (i.e., increase) in the Zemmouri-Boumerdes and Cap Djenet is remarkably opposite to that observed (i.e., decrease) during the coseismic deformation [see *Belabbes et al.*, 2009]. This can be explained by shallow afterslip below or above the area of coseismic slip on the fault surface since it produces both NW directed horizontal motion and subsidence. Hence, we obtain the range increase, consistent with the shallow afterslip model proposed by *Mahsas et al.* [2008]. Afterslip on fault sections of coseismic slip would give rise to uplift and range decrease, similarly to the coseismic motion. Considering the coseismic fault rupture parameters and satellite imaging geometry, the LOS velocity field largely depends on vertical movement as InSAR in this case can detect only 20–25% of NW horizontal displacements and about 90% of the vertical displacements.

4. Modeling Geodetic Data

[8] We investigate how a model of afterslip can explain the InSAR LOS velocity field and CGPS measurements of *Mahsas et al.* [2008]. Our inverse modeling is based on the boundary element software, Poly3Dinv [*Maerten et al.*, 2005] that predicts surface displacements due to dislocations on triangular faults buried in a linear elastic and homogeneous half-space with a damped least square minimization. The curved model fault dipping ~45° towards the south and trending N60°–65°E along the coast is deduced from coseismic SAR, GPS data, and coastal uplift measurements (Figure 2a) [*Belabbes et al.*, 2009]. The fault surface is discretized into triangular elements from surface down to the 20-km-depth. The distribution of reverse slip on triangular elements was then inverted with the scale-dependent smoothing operator of Poly3Dinv to avoid unphysical oscillatory slip, using the cumulative LOS change along the shoreline and re-estimated horizontal GPS displacements during ~7 years. We use time series provided by *Mahsas et al.* [2008] to recalculate horizontal GPS velocities taking into account the total displacements recorded in between the acquisition of the first Envisat image in July 2003, and the end of CGPS measurements in October 2005. Here, the GPS displacement rate for the next

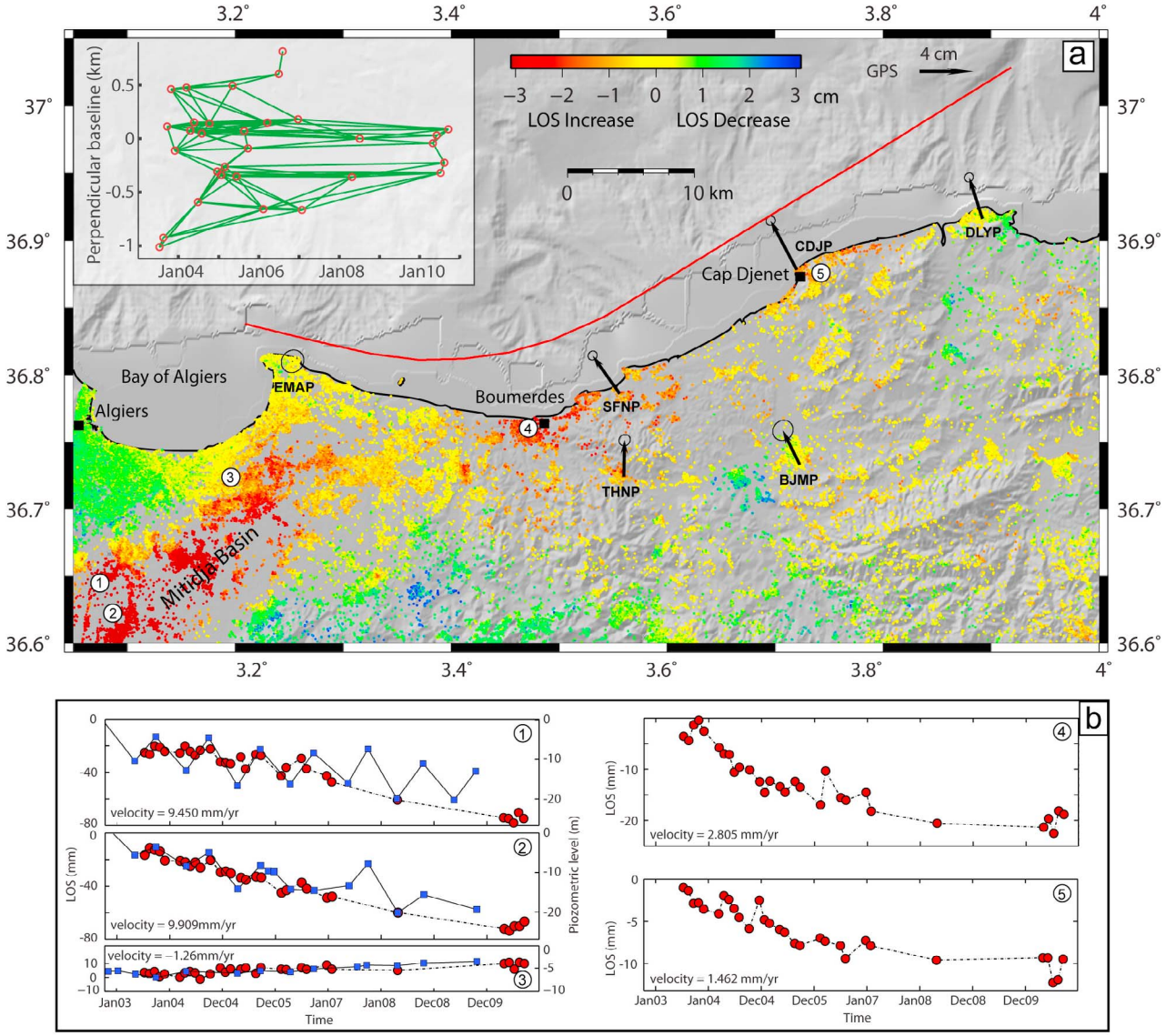

Figure 2. (a) Seven-year postseismic cumulative LOS range change following the 2003 Zemmouri earthquake calculated from 31 descending Envisat images on Track 65. Movements away from the satellite are shown with yellow to red colors and, those towards the satellite with yellow to blue. The black arrows with 95% confidence ellipses are 2.5-year cumulative postseismic GPS displacements from *Mahsas et al.* [2008]. Red line is the trace of the modeled fault on the sea floor. Numbers show the locations of time series plotted in Figure 2b. Inset is the baseline plot showing the interferogram pairs (green lines) between radar images (red circles). (b) Time series of InSAR data (red circles) and groundwater table measurements (blue squares [*Mimouni*, 2010]) in the study area. Note the strong correlation between water level fluctuations and InSAR phase changes in the Mitidja basin (plots 1 to 3). Postseismic deformation in the earthquake region (plot 4 and 5) is manifested by logarithmic decay in the InSAR time series.

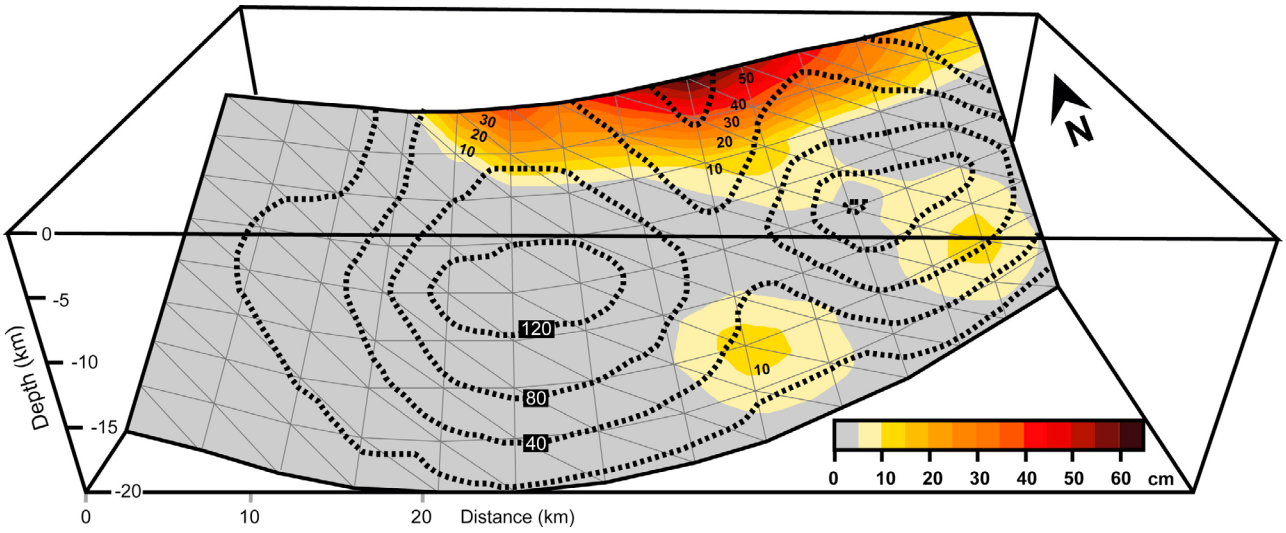

Figure 3. Color-coded postseismic afterslip distribution on the Zemmouri earthquake rupture. Black dashed lines show the coseismic slip distribution inferred by *Belabbes et al.* [2009]. The afterslip distribution inverted from InSAR and GPS data shows two patches of maximum slip (40 to 65 cm) along the upper sections of the fault (<5-km-depth) complementing the coseismic slip at deeper fault sections.

five years till the acquisition of the last Envisat image in September 2010 is assumed to be linear. We then run several inversions weighting the GPS and LOS data equally with 0 (rough) to 1 (smooth) smoothing factor to explore its effects on the location, magnitude of slip and misfit. Although the fit improves almost linearly for LOS data with decreasing smoothing factor and roughness (Figure 4b inset), at a certain point GPS data exhibit a higher misfit as the slip localizes further reaching 2 m maximum. The preferred model of slip distribution shown in Figure 3 is obtained with an optimum 0.4 smoothing factor for both data sets with 0.57 cm RMS misfit. As for all other models with different smoothing factors, the preferred model predicts up to 65 cm shallow afterslip localized mostly between 5-km-depth and surface. The weakly pronounced afterslip is distributed on two patches above the lobes of high coseismic slip. The coseismic slip deficit at the uppermost sections of the fault appears to be filled by the postseismic afterslip, indicating a complementary slip distribution also observed in other large earthquakes [*Reilinger et al.*, 2000]. The resolution tests shown in Figure S1 in the auxiliary material indicates that the InSAR data have an adequate resolution in constraining the shallow slip on the fault.[1] As illustrated in Figure 4, the fit between the model and InSAR data can be reasonably accepted. In contrast, the GPS fit in the south and east is poor and requires deeper slip on fault although the model predicts the overall northward displacements observed by GPS. The discrepancy between the modeled and observed GPS velocities and the InSAR data is probably partly due to much faster decays of the afterslip on the deeper sections of the fault. The estimated moment released for 7 years (2003–2010) is 4.1×10^{18} Nm (Mw = 6.34), ~28% higher than that estimated during the first 2.5 years [*Mahsas et al.*, 2008]. The cumulative postseismic moment release during 7 years may range between 15 to 25% of the coseismic moment release estimated from seismology and geodesy [*Delouis et al.*, 2004; *Belabbes et al.*, 2009].

5. Discussion and Conclusion

[9] Postseismic deformation associated with the Zemmouri earthquake from 2003 to 2010 is documented using Envisat data combined with 2.5-year GPS data. The broad spatial coverage and seven years of high-resolution SBI data provide a powerful constraint on the characteristics of postseismic deformation. The results reveal two lobes of relatively higher rate of surface deformation with 3.5 to 2 mm/yr LOS displacement in Boumerdes and Cap Djenet, respectively, as opposed to the coseismic uplift. Elastic dislocation modeling shows that these lobes can be adequately explained by shallow (<5 km) afterslip with up to 0.65 m displacement above the coseismic slip with 4.1×10^{18} Nm (Mw = 6.34) cumulative moment release. The coseismic and postseismic slip distributions are shown to be complementary implying that both types of surface deformation with the same fault model suggest well-constrained fault rupture parameters. The large amount of afterslip gives rise to additional static stress transfer onto the neighboring faults and affects previous Coulomb stress modeling [*Lin et al.*, 2011]. This also changes our perception of the seismic cycle characterization and suggests longer recurrence intervals for large earthquakes in the Algiers region.

[10] Three mechanisms are widely used to explain the postseismic deformation of numerous large and moderate earthquakes: (1) afterslip on the coseismic rupture plane [*Smith and Wyss*, 1968], (2) visco-elastic relaxation in the lower crust/upper mantle [*Pollitz et al.*, 2000], and (3) poro-elastic rebound [*Peltzer et al.*, 1998]. While in similar cases only one mechanism is claimed to have operated [*Freed*, 2007], in other examples several mechanisms are thought to contribute to postseismic deformation [*Hearn et al.*, 2009]. Following the 2003 Zemmouri thrust earthquake, the afterslip distribution is well constrained and appears to be the

[1]Auxiliary materials are available in the HTML. doi:10.1029/2012GL051344.

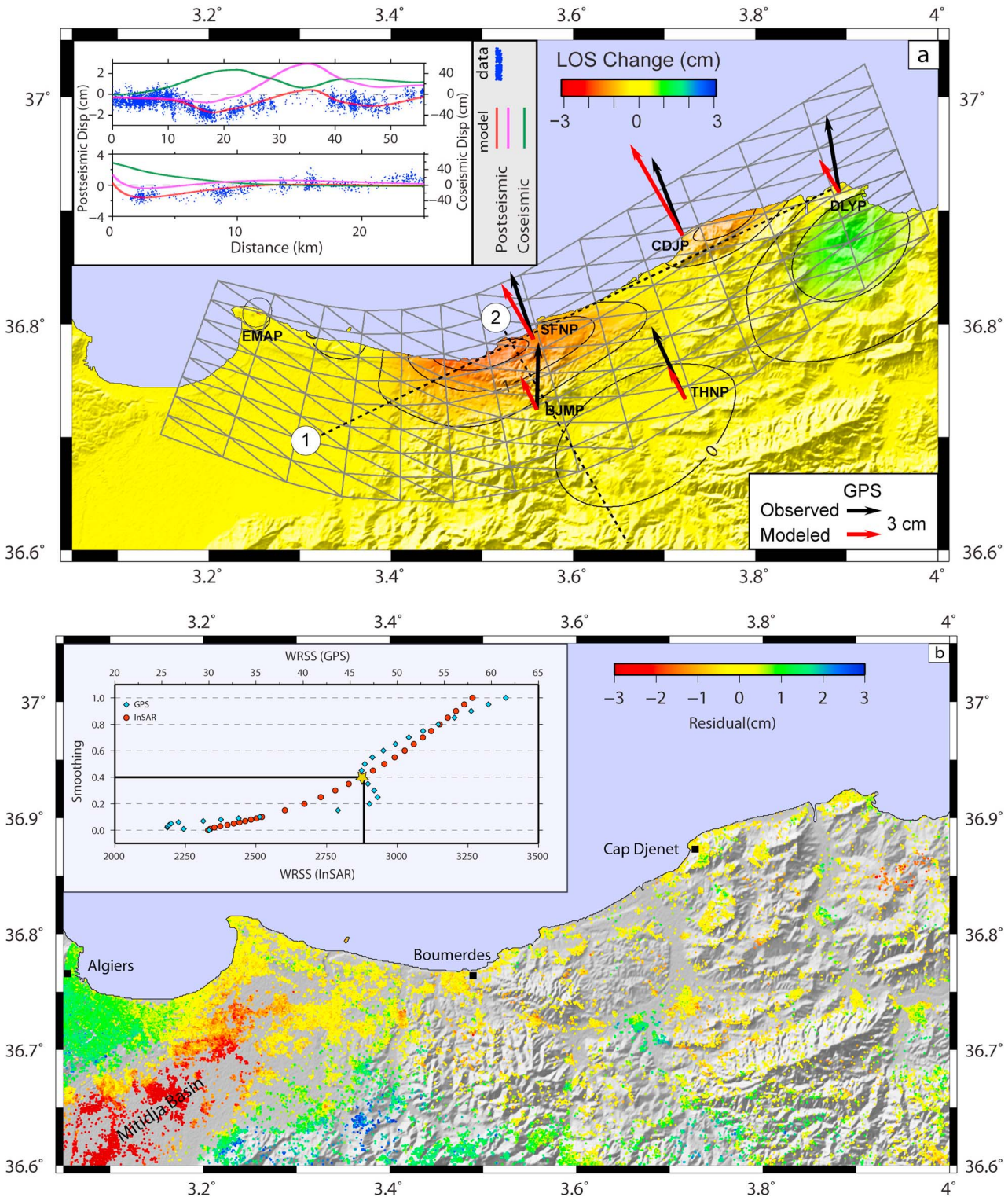

Figure 4. (a) Model of 7-year cumulative LOS surface deformation and GPS displacements predicted by the modeled slip distribution shown in Figure 3. The fault rupture projected to the surface is illustrated by the triangulated network; parallel and perpendicular profiles to the fault are located by number 1 and 2. Inset shows LOS change of modeled (red lines) and observed (blue dots) postseismic surface deformation, together with coseismic model (green lines [*Belabbes et al.*, 2009]). Pink lines show vertical component of the LOS change predicted by the model. (b) Residual LOS velocity field. Inset shows the trade-off between misfit (weighted residual sum of squares) and the smoothing factor in the InSAR and GPS data inversion. An optimum solution can be obtained with a 0.4 smoothing factor.

most significant mechanism of the postseismic deformation mostly at shallow depths. Part of the postseismic deformation can be due to poro-elastic and/or visco-elastic relaxation in the lithosphere (Figures S2a and S2b). Postseismic deformation of the Chi-Chi thrust earthquake (Mw 7.7) obtained from GPS measurements over a 15-month period are better explained by afterslip than viscoelastic relaxation [*Hsu et al.*, 2007]. In the Zemmouri earthquake, the visco-elastic relaxation model [*Mahsas et al.*, 2008] predicts the subsidence observed in the InSAR results. The model however fails to explain the far field horizontal motions observed with GPS and the two-lobe pattern observed by SBI. The visco-elastic contribution to the observed surface deformation remains unclear (Figure S2a). On the other hand, the poro-elastic rebound is a fairly rapid response [*Riva et al.*, 2007], and its contribution is likely to be small since the first SAR image was taken ~6 weeks after the earthquake (Figure S2b).

[11] **Acknowledgments.** This work was performed thanks to the ESA grant for ENVISAT images through the C1P-2532 project. Esra Cetin benefited from the EGIDE-Eiffel grant (721450B) during the completion of this work. We are thankful to A. Hooper for providing access to StaMPS software tools and to Samir Belabbes and Noel Gourmelen for discussions. We thank Tim Wright and an anonymous reviewer for improving a previous version of the paper.

[12] The Editor thanks Tim Wright and an anonymous reviewer for assisting with the evaluation of this paper.

References

Ayadi, A., C. Dorbath, F. Ousadou, S. Maouche, M. Chikh, M. Bounif, and M. Meghraoui (2008), Zemmouri earthquake rupture zone (Mw 6.8, Algeria): Aftershocks sequence relocation and 3D velocity model, *J. Geophys. Res.*, *113*, B09301, doi:10.1029/2007JB005257.

Belabbes, S., C. Wicks, Z. Cakir, and M. Meghraoui (2009), Rupture parameters of the 2003 Zemmouri (Mw 6.8), Algeria, earthquake from joint inversion of interferometric synthetic aperture radar, coastal uplift, and GPS, *J. Geophys. Res.*, *114*, B03406, doi:10.1029/2008JB005912.

Berardino, P., G. Fornaro, R. Lanari, and E. Sansosti (2002), A new algorithm for surface deformation monitoring based on small baseline differential SAR interferograms, *IEEE Trans. Geosci. Remote Sens.*, *40*, 2375–2383, doi:10.1109/TGRS.2002.803792.

Delouis, B., M. Vallee, M. Meghraoui, E. Calais, S. Maouche, K. Lammali, A. Mahsas, P. Briole, F. Benhamouda, and K. Yelles (2004), Slip distribution of the 2003 Boumerdes-Zemmouri earthquake, Algeria, from teleseismic, GPS, and coastal uplift data, *Geophys. Res. Lett.*, *31*, L18607, doi:10.1029/2004GL020687.

Freed, A. M. (2007), Afterslip (and only afterslip) following the 2004 Parkfield, California, earthquake, *Geophys. Res. Lett.*, *34*, L06312, doi:10.1029/2006GL029155.

Hearn, E. H., S. McClusky, S. Ergintav, and R. E. Reilinger (2009), Izmit earthquake postseismic deformation and dynamics of the North Anatolian Fault Zone, *J. Geophys. Res.*, *114*, B08405, doi:10.1029/2008JB006026.

Hooper, A. (2008), A multi-temporal InSAR method incorporating both persistent scatterer and small baseline approaches, *Geophys. Res. Lett.*, *35*, L16302, doi:10.1029/2008GL034654.

Hsu, Y., P. Segall, S. Yu, L. Kuo, and C. Williams (2007), Temporal and spatial variations of post-seismic deformation following the 1999 Chi-Chi, Taiwan earthquake, *Geophys. J. Int.*, *169*, 367–379, doi:10.1111/j.1365-246X.2006.03310.x.

Kampes, B., and S. Usai (1999), Doris: The Delft Object-oriented Radar Interferometric software, paper presented at ITC 2nd ORS Symposium, Int. Inst. for Geoinf. Sci. and Earth Obs., Enschede, Netherlands.

Lin, J., R. Stein, M. Meghraoui, S. Toda, A. Ayadi, C. Dorbath, and S. Belabbes (2011), Stress transfer among en echelon and opposing thrusts and tear faults: Triggering caused by the 2003 Mw = 6.9 Zemmouri, Algeria, earthquake, *J. Geophys. Res.*, *116*, B03305, doi:10.1029/2010JB007654.

Maerten, F., P. Resor, D. Pollard, and L. Maerten (2005), Inverting for slip on three dimensional fault surfaces using angular dislocations, *Bull. Seismol. Soc. Am.*, *95*(5), 1654–1665, doi:10.1785/0120030181.

Mahsas, A., K. Lammali, K. Yelles, E. Calais, A. Freed, and P. Briole (2008), Shallow afterslip following the 2003 May 21, Mw = 6.9 Boumerdes earthquake, Algeria, *Geophys. J. Int.*, *172*, 155–166, doi:10.1111/j.1365-246X.2007.03594.x.

Maouche, S., M. Meghraoui, C. Morhange, S. Belabbes, Y. Bouhadad, and H. Haddoum (2011), Active coastal thrusting and folding, and uplift rate of the Sahel Anticline and Zemmouri earthquake area (Tell Atlas, Algeria), *Tectonophysics*, *509*, 69–80, doi:10.1016/j.tecto.2011.06.003.

Meghraoui, M., S. Maouche, B. Chemaa, Z. Cakir, A. Aoudia, A. Harbi, P. Alasset, A. Ayadi, Y. Bouhadad, and F. Benhamouda (2004), Coastal uplift and thrust faulting associated with the Mw = 6.8 Zemmouri (Algeria) earthquake of 21 May, 2003, *Geophys. Res. Lett.*, *31*, L19605, doi:10.1029/2004GL020466.

Mimouni, O. (2010), Pollutions des eaux de la région d'Alger, leurs impacts sur l'environnement et les risques majeurs, report, Univ. des Sci. et Tech. Houari Boumediene, Algiers.

Morel, J. L., and M. Meghraoui (1996), Goringe-Alboran-Tell tectonic zone: A transpression system along the Africa-Eurasia plate boundary, *Geology*, *24*, 755–758, doi:10.1130/0091-7613(1996)024<0755:GATTZA>2.3.CO;2.

Nocquet, J. M., and E. Calais (2004), Geodetic measurements of crustal deformation in the western Mediterranean and Europe, *Pure Appl. Geophys.*, *161*, 661–681, doi:10.1007/s00024-003-2468-z.

Peltzer, G., P. Rosen, F. Rogez, and K. Hudnut (1998), Poro-elastic rebound along the Landers 1992 earthquake surface rupture, *J. Geophys. Res.*, *103*(B12), 30,131–30,145, doi:10.1029/98JB02302.

Pollitz, F. F., G. Peltzer, and R. Bürgmann (2000), Mobility of continental mantle: Evidence from postseismic geodetic observations following the 1992 Landers earthquake, *J. Geophys. Res.*, *105*, 8035–8054, doi:10.1029/1999JB900380.

Reilinger, R. E., et al. (2000), Coseismic and postseismic fault slip for the 17 August 1999, M = 7.5, Izmit, Turkey earthquake, *Science*, *289*(5484), 1519–1524, doi:10.1126/science.289.5484.1519.

Riva, R. E. M., A. Borghi, A. Aoudia, R. Barzaghi, R. Sabadini, and G. F. Panza (2007), Viscoelastic relaxation and long-lasting after-slip following the 1997 Umbria-Marche (central Italy) earthquakes, *Geophys. J. Int.*, *169*, 534–546, doi:10.1111/j.1365-246X.2007.03315.x.

Rosen, P., S. Hensley, G. Peltzer, and M. Simons (2004), Updated repeat orbit interferometry package released, *Eos Trans. AGU*, *85*(5), 47, doi:10.1029/2004EO050004.

Smith, S. W., and M. Wyss (1968), Displacement on the San Andreas fault subsequent to the 1966 Parkfield earthquake, *Bull. Seismol. Soc. Am.*, *58*(6), 1955–1973.

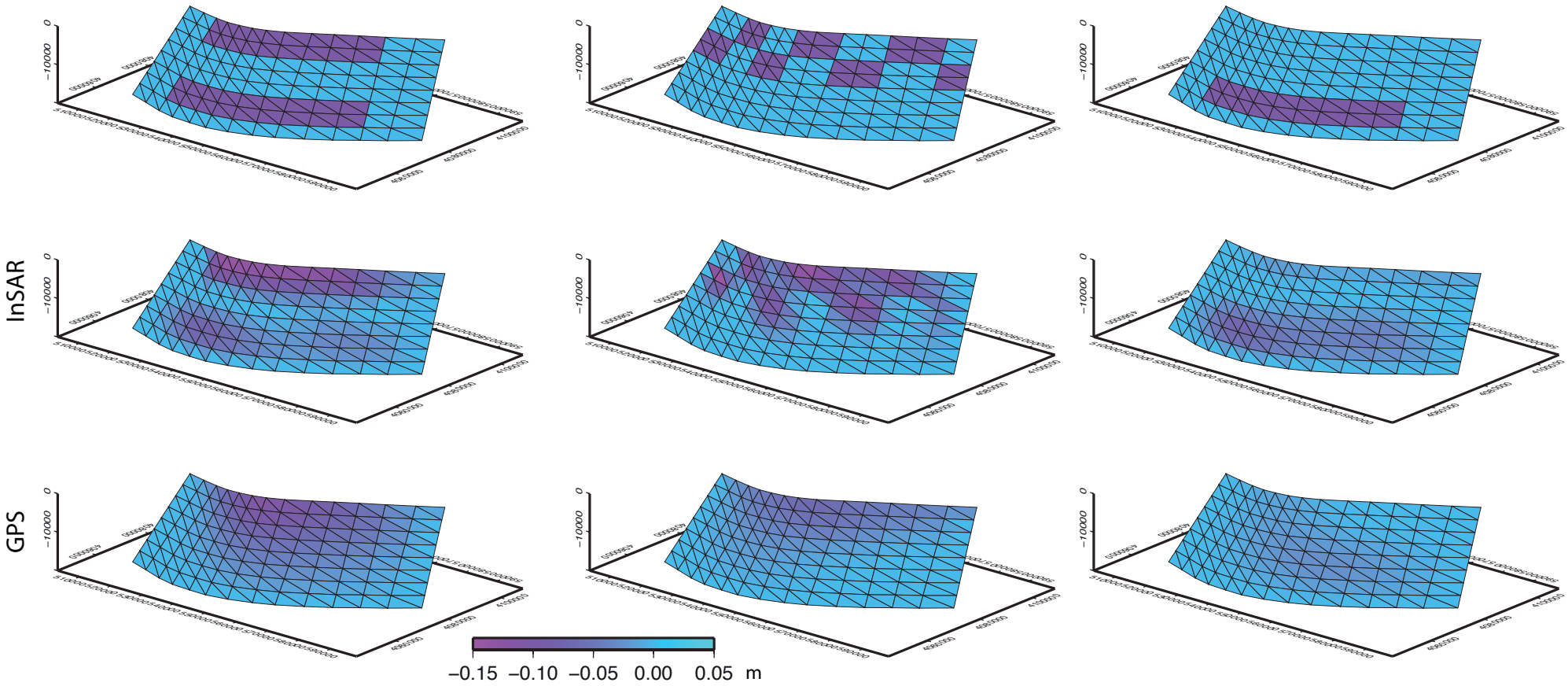

Figure S1. Resolution test using check-box approach with 0.10 m slip at different depths for each cell.

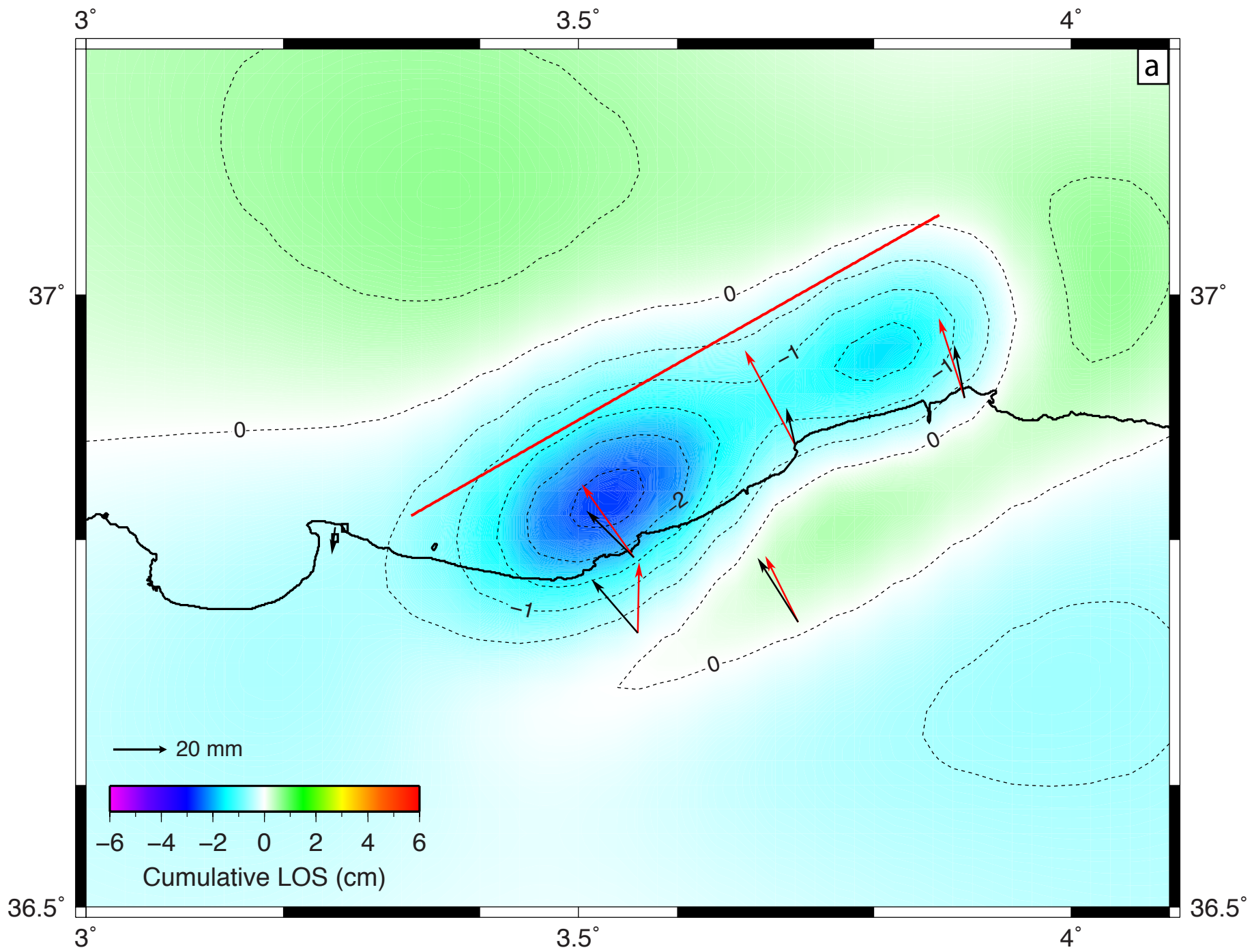

Figure S2. Visco-elastic deformation model.

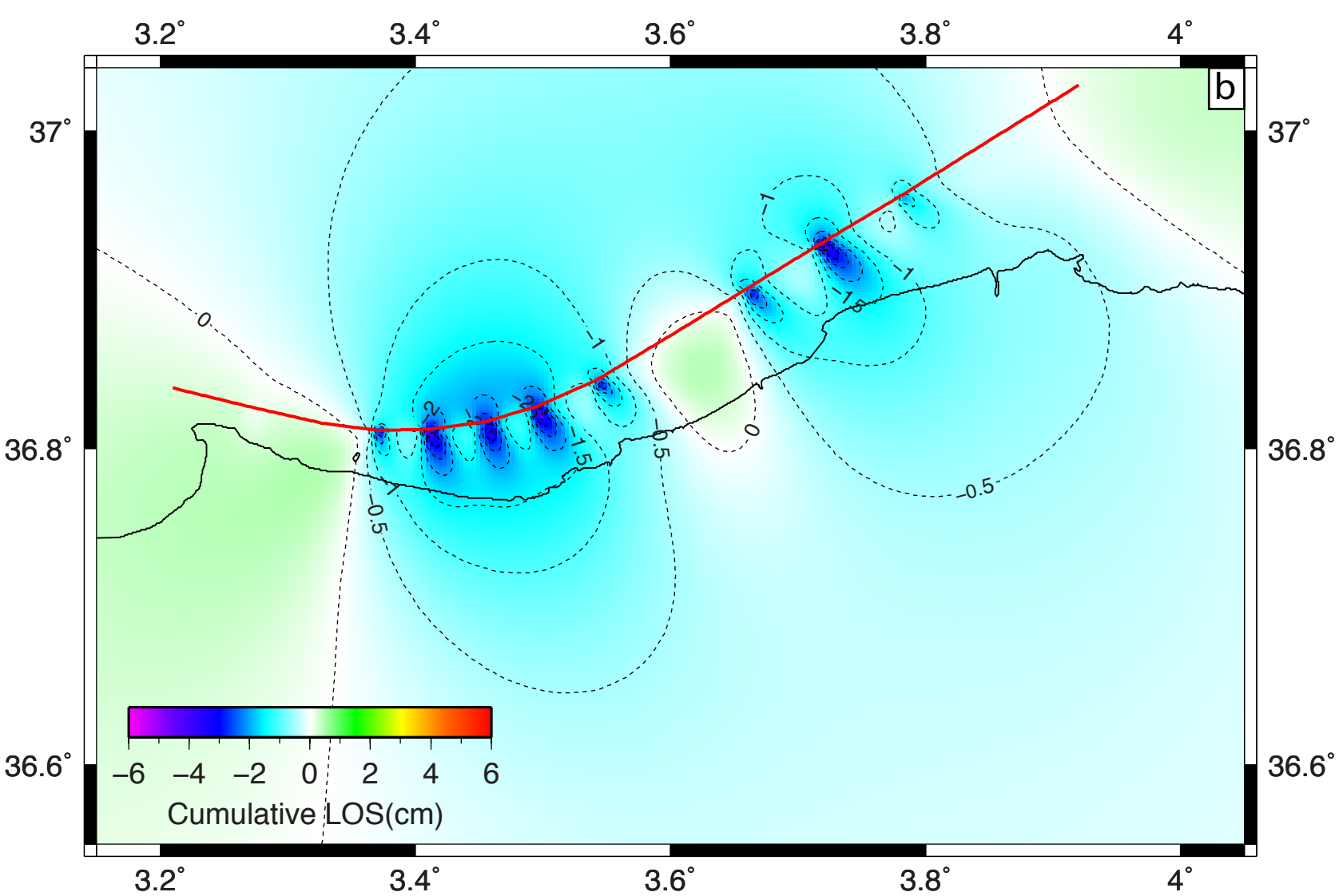

Figure S2. Poro-elastic deformation model.